Published in final edited form as:
Epilepsia. 2011 March ; 52(3): 497–506. doi:10.1111/j.1528-1167.2010.02912.x.

STEP Regulation of Seizure Thresholds in the Hippocampus

Gloster Aaron[1,3], **Stephen Briggs**[1,3,4], **Jeffrey Walker**[1], **Kemal Asik**[1], **Paul Lombroso**[2], and **Janice Naegele**[1]

[1] Department of Biology, Program in Neuroscience and Behavior, Wesleyan University, Middletown, Connecticut 06459

[2] Child Study Center, Yale University School of Medicine, New Haven, Connecticut, 06520

Summary

Purpose—To investigate whether STriatal Enriched protein tyrosine Phosphatase (STEP) influences ictogenesis.

Methods—STEP knockout mice were compared to wild-type (WT) mice in pilocarpine-induced seizures. Hippocampal slices were also prepared from these two mouse populations, allowing the examination of ictal-like stimulation in these slices using calcium imaging and electrophysiological recordings.

Results—To examine seizure thresholds, increasing doses of pilocarpine were administered to adult mice and seizures were scored behaviorally. Significantly fewer STEP knockout mice developed seizures that progressed to the stage of status epilepticus compared to WT mice. To examine potential differences in neural circuits that might account for this finding, seizure-like activity was induced in hippocampal slices. Electrical stimulation of the hippocampal-entorhinal cortex pathway in STEP knockout mice resulted in less activation of the dentate granule cell layer, but greater activation of the hilus in STEP knockouts, compared with heterozygous slices.

Conclusions—STEP deficiency is associated with higher seizure thresholds. The locus of these effects appears to include the dentate gyrus granule cell layer and hilus.

Keywords

hilus; inhibitory interneurons; glutamatergic mechanisms; pilocarpine; perforant path; status epilepticus

Introduction

In humans and rodents, a single, severe period of status epilepticus (SE) can result in the emergence of spontaneous epileptic seizures and temporal lobe epilepsy (TLE). The appearance of spontaneous seizures often occurs after a latent period that may range from weeks to years. Epileptogenesis potentially involves the loss of inhibitory synapses onto granule cells, as patients and rodents with TLE often exhibit hippocampal sclerosis and pronounced loss of interneurons in the dentate gyrus (Mathern et al., 1996; Kobayashi and

Correspondence to: Gloster Aaron, Ph.D. Department of Biology, Hall-Atwater Labs, Lawn Avenue, Middletown, CT 06459, Phone: 860 685-3197, Fax: 860 685-3279, gaaron@wesleyan.edu.
[3]These authors contributed equally to the paper.
[4]Current address: Albert Einstein College of Medicine of Yeshiva University, Jack and Pearl Resnick Campus 1300 Morris Park Avenue, Bronx, NY 10461.

None of the authors has any conflict of interest to disclose.

Buckmaster, 2003). Additionally, synaptic reorganization in the dentate gyrus appears to contribute to altered network properties causing spontaneous seizures (Thind et al., 2010).

A previous study led to the hypothesis that **ST**riatal **E**nriched protein tyrosine **P**hosphatase (STEP) significantly modulates survival of hippocampal interneurons in CA1-3 and the hilus in response to SE (Choi et al., 2007). STEP is enriched in neurons in the striatum, hippocampus, cortex, amygdala, nucleus accumbens and other regions of the CNS (Lombroso et al., 1993; Boulanger et al., 1995; Pelkey et al., 2002). The current model of STEP function is that it opposes the development of synaptic strengthening by dephosphorylating regulatory tyrosine residues in its substrates, which include proteins involved in synaptic plasticity and intracellular signaling. STEP dephosphorylates and inactivates the key signaling molecules ERK1/2, p38, and Fyn, and has also been shown to dephosphorylate and induce internalization of the ionotropic glutamate receptors GluN1/GluN2B and GluA1/GluA2 (Snyder et al., 2005; Zhang et al., 2008).

In mice and rats, intraperitoneal administration of appropriate doses of the muscarinic agonist pilocarpine can induce SE (Turski et al., 1983a). Depending on the duration and severity of SE, the sequelae can include neurodegeneration and astrogliosis in the hippocampus and temporal lobes. Days to weeks after prolonged SE, an epileptic disease state emerges as spontaneous seizures develop (Turski et al., 1983b; Loscher, 2002). As these patterns of neuronal damage are similar to those found in patients with temporal lobe epilepsy, pilocarpine-induced SE is considered a model of severe temporal lobe epilepsy.

STEP-expressing neurons in the hilus and area CA1 undergo excitotoxic cell death following pilocarpine-induced SE. The vulnerability of these neurons to seizures was mitigated by disrupting STEP functions in these cells, providing evidence for a possible role for STEP in excitotoxic neuronal cell death (Choi et al., 2007). STEP is expressed in a class of somatostatin-positive, GABAergic interneurons in the hilus (Choi et al., 2007). These interneurons are also known as **H**ilar **I**nterneurons whose axon ramifies in the **P**erforant **P**ath field (HIPP) (Han et al., 1993), and their main source of excitatory input are the mossy fibers originating from the GCL (Acsady et al., 1998). HIPPs produce the neuropeptide somatostatin, which is released from synaptic terminals during bursts of activity and may provide anti-epileptic properties (Tallent and Siggins, 1999; Baratta et al., 2002). HIPPs are also characterized by their axonal innervation patterns that target the same field as the perforant path axons, that is, the dendrites of dentate granule cells. Thus, HIPPs provide substantial feedback inhibition to the granule cells (Buckmaster et al., 2002).

Hilar interneurons, including HIPPs, are especially vulnerable to SE (Santhakumar et al., 2001; Buckmaster and Jongen-Relo, 1999), as well as other forms of epileptogenic trauma such as concussion (Lowenstein et al., 1992) and ischemia (Freund et al., 1990; Bering and Johansen, 1993; Johansen et al., 1987). These and other studies suggest that loss of the HIPP subtype of GABAergic interneuron is a causal factor in epileptogenesis, as degeneration of these interneurons removes an important brake on seizure generation, contributing to the development of spontaneous, recurrent seizures. There is much evidence to support this idea, including studies showing that the relative numbers of HIPPs are greatly reduced in humans who have suffered temporal lobe epilepsy (de Lanerolle et al., 1989; Mathern et al., 1995; Sloviter, 1987; Robbins et al., 1991).

Given the prevalence of STEP in hilar interneurons, we tested the hypothesis that a deficiency of the STEP protein would increase resistance to the development of SE in the pilocarpine model. Our results show that a significant number of STEP deficient mice exhibit a seizure-resistant phenotype. One potential mechanism for the resistance of STEP knockout mice to pilocarpine-induced SE is reduced excitability of GCL neurons in STEP

KO mice. Our analysis of GCL granule cell responses in WT vs. STEP KO mouse hippocampal slices suggests larger hyperpolarizing responses in STEP KO vs. WT granule cells. These novel findings suggest that STEP deficiency in mice is linked to enhanced feedback inhibition onto the GCL neurons. Taken together, these findings suggest that STEP inhibitors may be novel targets for seizure resistance therapies.

Methods

Mice

STEP WT and STEP KO mice were maintained on the C57Bl/6 inbred strain from Charles River Labs and were obtained from heterozygous breedings in the Wesleyan University Animal Facility, a pathogen free environment. The KO was originally generated using homologous recombination to remove a portion of the STEP gene, which included the catalytic site, and the knockout mice were generated on the 129 background at Pfizer, Inc. The strain was subsequently crossed into the C57Bl/6 strain (Charles River) and backcrossed for 7 generations. The WT, KO and heterozygous (HT) genotypes are fertile and visibly indistinguishable. Furthermore, there were no gross anatomical differences between genotypes in cresyl violet stained brain sections. Immunoblot analyses showed that no STEP protein is expressed in the KO, while the HT expresses 50% of the STEP protein levels heterozygote mice for any of our measures. The genotypes of the mice used for all experiments were confirmed by polymerase chain reaction using primers for STEP as described previously (Venkitaramani et al., 2009). All experiments involving the use of animals were in compliance with the guidelines provided by the Wesleyan University Institutional Animal Care and Use Committee and NIH.

Pilocarpine-induced SE

Adult male and female mice, weighing between 18 and 22 grams and 6–8 week of age were used. Seizures were pharmacologically induced by systemic injections of pilocarpine (280–320 mg/kg, i.p., Sigma, St. Louis, MO, U.S.A.) diluted in sterile 0.9% saline. To block the effects of pilocarpine in the peripheral nervous system, atropine methyl nitrite (1 mg/kg, i.p., Sigma) was injected 30 minutes prior to pilocarpine. Mice displayed seizure activity that was behaviorally scored, by a pair of observers using the a modified Racine scale (Shibley and Smith, 2002). The measurements included the latency to and number of seizure events before reaching SE. Typically, four to six seizure events were observed before the mice exhibited SE, defined as continuous motor seizures involving head bobbing and full body tremors. Pilocarpine was administered between 10 AM – 12 PM to minimize differences in hormonal milieu due to circadian rhythms.

Preparation of hippocampal formation slices

Young adult male and female mice (ages postnatal 18 to 22 days) were injected with ketamine/xylazine (120 mg/kg ketamine-10 mg/kg xylazine) intraperitoneally. Once unconscious and unresponsive to noxious stimuli, they were decapitated and brains were quickly removed and placed in high-sucrose ice-cold artificial cerebral spinal fluid (ACSF). The composition of high sucrose ACSF is (in mM): 222 sucrose, 27.1 sodium bicarbonate, 1.5 sodium phosphate, 2.6 potassium chloride, 1 calcium chloride, 3 magnesium sulfate. Hippocampal slices were modeled from a previous study (Rafiq et al., 1993): The brain was removed and blocked on a ramp, so that the dorsal side of brain was cut at a 12 degree angle (cutting at increasing depth from the rostral to caudal direction). This cut dorsal side of the brain was glued to the vibratome stage. Horizontal slices were cut from this blocked brain with a vibratome (Leica VT1000S) at 350 micrometer thicknesses, while bathed in ice-cold high sucrose ACSF. Slices were then transferred to warm (37°C), oxygenated ACSF containing high magnesium and low calcium to reduce spontaneous activities and, thus,

neurotoxicity (composition of this ACSF (in mM): 126 sodium chloride, 26 sodium bicarbonate, 1.1 sodium phosphate, 10 dextrose, 3 potassium chloride, 3 magnesium sulfate, 1 calcium chloride). The slices were then allowed to equilibrate to room temperature. During recordings, the slices were transferred to a recording chamber and perfused with oxygenated recording ACSF (in mM): 1 magnesium sulfate, 1.5 calcium chloride, 4.5 potassium chloride. This recording ACSF increases excitability of the circuitry by reducing divalent cations and increasing extracellular potassium (Sanchez-Vives and McCormick, 2000).

Imaging

A 100 μl solution of calcium dye was prepared prior to slicing: 50 μg of fura-2AM, 2 μl pluronic acid, 48 μl DMSO, and 50 μl ACSF. This solution was divided equally among 4–5 hippocampal slices and directly applied with a pipette to the surface of each slice. The slices were then left undisturbed to incubate in darkness for 1 hour. Fluorescence was observed in loaded neurons using 380 nm wavelength excitation light (ultraviolet), while collecting the emitted 510 nm light. Movies were made with a slit-disk spinning confocal unit (Olympus Disk-Scan and BX51WI upright microscope), a Hamamatsu C39100-12 CCD camera, and an acquisition program, SimplePCI (Cimaging). Frames were captured using a 20X objective at a rate of 5 Hz and spatial resolution of 256×256 pixels using SimplePCI software (Compix). Calcium imaging experiments such as these are reliable measures of neuronal action potential activity (Smetters et al., 1999; MacLean et al., 2005; Aaron and Yuste, 2006).

Electrophysiology

Extracellular stimulation of the Schaffer collaterals was performed with a concentric bipolar electrode (Frederick Haer) placed directly on the Schaffer collaterals. For each slice, the 60 Hz tetanic stimulation was delivered three times, with 10 minutes of rest in between each stimulation. For each slice, the tetanic stimulation was repeated twice with a 10-minute interstimulus interval, for a total of three tetanic stimuli per slice. Some experiments also included extracellular recordings performed with a 3 MΩ pipette filled with ACSF to verify the large responses seen in the GCL.

Whole cell patch clamp recordings

Individual GCL granule cells were identified under IR-DIC optics. Whole-cell voltage clamp recordings were performed using 6–9 MΩ pipettes containing a cesium gluconate solution (Cs-gluc) that blocked potassium channels, allowing us to voltage clamp the cell at +10 mV without substantial leak current. This technique reduces EPSCs as this potential is close to the reversal potential of EPSCs, and it increases the driving force for IPSCs, delivering high signal-to-noise recordings of IPSCs. The Cs-gluc solution, in (mM): 135 gluconic acid, 135 CsOH, 1 EGTA, 8 MgCl, 0.1 CaCl2, 10 HEPES, 2 Mg-ATP, 0.3 Na-GTP, 11 biocytin.

Cell-attached recordings

Individual GCL granule cells were identified under IR-DIC optics, and they were recorded with pipette electrodes (6–9 M MΩ) containing 140 mM NaCl. Giga-ohm seals were formed between the electrodes and granule cells. In this configuration, rough measurements of voltage changes in the cell can be achieved in current-clamp mode through the resistance of the patch of membrane between the electrode and intracellular space (Perkins, 2006).

Analyses

Measurement of responses in calcium imaging recordings: for each neuron we defined the fluorescence change over time as $\Delta F/F = (F_1 - F_0)/F_0$, expressed in %, where F_1 is

fluorescence at any time point, and F_0 is the baseline fluorescence measured during the first 3-seconds at the beginning of each trial. Neurons were identified and their respective borders outlined using custom-built macros in Matlab (Mathworks). For each identified neuron, the ΔF/F was further adjusted according to the difference between the ΔF/F measured within the neuron's borders minus the ΔF/F measured in the immediate background of the neuron (a halo region around the neuron equal to the area of the neuron). This was done to distinguish the neuronal response from background response. **Mean peak fluorescence**: For each neuron, the 2-second interval beginning with the initiation of the 1-second tetanic stimulus is labeled as the stimulus interval. The largest ΔF/F frame during the 2-second stimulus interval was used to center a 1-second interval whose mean was taken as the peak fluorescence (as in Fig. 3Bi). Given our sampling rate, this peak fluorescence is the mean of 5 frames. The mean peak fluorescence from a stimulus in a slice was then taken as the mean fluorescence of each peak measured in each neuron from the group (i.e., GCL or hilus). **Proportion of responses:** A neuron qualified as responding to the tetanic stimulation if the mean - ΔF/F during the 2-second stimulus interval was greater than 1 standard deviation of mean of the ΔF/F measured during the baseline. The proportion, defined as the number of responding neurons/all neurons in GCL or hilus, was calculated to allow comparisons of proportions (as in Fig. 3Bii).

Electrophysiological measurements

For each voltage clamp and cell-attached recording, the mean of the 3-seconds of baseline before the stimulus, was subtracted from the mean of the 1-second stimulus, yielding the mean baseline subtracted 1-second response for each recording.

Both WT mice and STEP KO heterozygote mice were used as the control mouse population in this experiment as no significant differences were found between WT and the heterozygote mice for any of our measures. This result is supported by a previous study (Venkitaramani et al., 2009). All means are listed as the mean ± standard error.

Results

We first conducted dose-response experiments to test for differences in thresholds for pilocarpine-induced SE in WT and STEP KO mice. With doses of pilocarpine at 300 or 320 mg/kg, we found that 41/55 WT mice entered SE (75%), compared to 10/29 STEP KO mice (35%) ($p<0.001$, Chi-square test, Fig. 1). These results demonstrated that the STEP KO mice were resistant to the ictogenic effects of pilocarpine.

We next examined whether there were electrophysiological differences between WT and STEP KO mice that could explain the differences in the required doses of pilocarpine needed to induce SE. We employed the mouse entorhinal cortex-hippocampal slice preparation, where repetitive ictal-like extracellular stimulations of the Schaffer collaterals cause potentiation of neuronal responses in the GCL (Rafiq et al., 1993). The Schaffer collaterals were stimulated with extracellular tetanic stimulation, producing an ictal-like burst of activity that propagated throughout the slice. We measured this activity in the hilus and dentate gyrus simultaneously using calcium imaging (Fig. 2). We obtained these recordings in both STEP KO and WT slices, and included those slices where a measurable response to the stimulus was observed in the GCL or hilus.

We used calcium imaging to confirm a significant increase among WT slices in the mean peak fluorescence of the GCL measured during stimulus 3 versus stimulus 1 ($p < 0.03$, sign test, Fig. 3Ai and Bi) (Rafiq et al., 1993). In contrast, we observed no such potentiation between stimulus 1 and 3 in the hilus ($p = 0.81$, sign test, Fig. 3Bi) from either the WT or STEP KO slices. Furthermore, the mean peak fluorescence measured in the GCL from STEP

KO slices was significantly less than that from WT slices, when comparing responses from stimulus 3 ($p < 0.05$, Mann-Whitney U-test, Fig. 3Aii and Bii). These results show that there is less potentiation in the STEP KO slices, such that after three tetanic stimuli, the peak response in the GCL was significantly lower in STEP KO compared to WT hippocampal slices.

Interestingly, the results were markedly different in the hilus of STEP KO slices, where the proportion of neurons responding to stimulus 1 was significantly greater in the STEP KO compared to WT slices ($n = 16$ WT slices and $n = 18$ STEP KO slices, $p < 0.04$, t-test, Fig. 3Bii). As shown, there were no apparent differences in the GCL (Fig. 3Bii) with regard to this metric.

These differences were found despite the fact that the numbers of neurons identified with the calcium fluorophore fura-2 were equivalent for the STEP KO vs. WT slices. The numbers of neurons imaged in the GCL of WT and STEP KO slices were 137 ± 6.7 vs. 148 ± 7.3 imaged neurons, respectively ($p = 0.49$, Mann-Whitney U-test). The numbers of neurons imaged in the hilus for WT and STEP KO slices were 118 ± 7.7 vs. 118 ± 6.3 neurons, respectively ($p = 0.95$, Mann-Whitney U-test; $n = 16$ WT slices and $n=18$ STEP KO slices). Therefore, the results presented here demonstrate significantly different levels of responsiveness in both the GCL and hilus of WT vs. STEP KO slices, despite no differences in the mean number of neurons that were imaged in these slices.

The data presented are consistent with the hypothesis that HIPP inhibitory input to GCL dendrites is stronger in STEP KO mice. We investigated this hypothesis further by recording IPSCs in single granule cells during the calcium imaging experiments. The IPSCs recorded were most likely GABA-A ionotropic currents, as the electrodes contained a cesium gluconate solution that blocked potassium conductances, including GABA-B activated potassium conductances, and the voltage clamp was maintained at +10 mV, near the reversal potential for glutamatergic currents. Recordings of IPSCs were made from 23 cells in 11 WT mice, and 26 cells in 10 STEP KO mice. We measured the latencies of IPSCs in those cases where we could clearly identify the rising phase of the first IPSC in the train. Latencies in these cases were measured from the stimulus artifact from the first shock to the beginning of the IPSC, and there were no difference between STEP KO and WT in these latency measurements (13.7 ± 1.2 msec, $n = 12$; 13.7 ± 0.5 msec, $n = 16$; STEP KO and WT, respectively).

In comparing amplitudes of IPSCs between stimulus 3 with stimulus 1, we measured a significant increase from WT mice (Fig. 4), similar to the increase in putative granule cell action potential activity measured during calcium imaging (Fig. 3). As shown in Figure 4, there was no significant difference in IPSC amplitudes when comparing WT vs. STEP KO mice, contrary to the proposed hypothesis of increased GABAergic activity in STEP KO mice.

We then used cell-attached recordings to measure granule cell responses. We were able to record strong responses to the stimulus (Fig. 5), and we were also able to measure potentiation of responses during the 3 stimulus trials (Fig. 5B). A total of 7 cells from 4 STEP KO mice and 12 cells from 4 WT mice were successfully recorded with this technique. We observed potentiation (as seen in Fig. 5B) from 3 WT cells and 1 STEP KO cell.

Interestingly, the majority of granule cell responses were hyperpolarizing (Fig. 6). Some of these hyperpolarizing responses were large and long-lasting, often outlasting the duration of the stimulus itself. In comparing all hyperpolarizing responses from WT and STEP KO recordings, we found a significantly larger mean hyperpolarizing response in STEP KO vs.

WT recordings (−8.5 ± 1.7 vs. −3.8 ± 0.53 mV, n = 15 vs. 25 recordings, respectively, $p<0.04$, Mann-Whitney U-test). These results suggest a stronger stimulus-evoked inhibitory response in STEP KO granule cells, in contrast to observations made with voltage clamp experiments.

Discussion

The results shown in this series of experiments lead to a number of conclusions: (1) STEP KO mice are less sensitive to the ictogenic effects of pilocarpine as they require higher doses to reach SE; (2) the GCLs of STEP KO mice have a reduced excitability, especially as measured during repetitive ictal-like stimulations; and (3) neurons in the hilus of STEP KO mice demonstrate enhanced excitability during repetitive ictal-like stimulation, compared to WT mice. These neurons may be the source of enhanced inhibition to the dendrites of GCL granule cells in STEP KO mice.

STEP

STEP has been shown previously to regulate synaptic strengthening, glutamate receptor trafficking, and cell death (Braithwaite et al., 2006b). The novel finding reported here is that STEP deficiency is correlated with a seizure-resistant phenotype, both in the pilocarpine model of temporal lobe epilepsy and in hippocampal slices subjected to tetanic stimulation. Substrates of STEP include the extracellular-signal regulated kinase 1/2 (ERK1/2), the stress-activated protein kinase p38, and the Src kinase family member Fyn (Paul et al., 2003; Munoz et al., 2003; Nguyen et al., 2002).

STEP dephosphorylates these kinases at regulatory tyrosine residues within their activation loop and inactivates them. STEP dephosphorylates the NMDAR subunit GluN2B at tyr^{1472}, which promotes internalization of the GluN1/GluN2B receptor complex (Kurup et al., 2010b; Snyder et al., 2005). STEP also mediates internalization of GluA1/GluA2-containing AMPARs following activation of group I metabotropic glutamate receptors, although whether this is due to a direct dephosphorylation of GluA2 remains to be determined (Zhang et al., 2008). STEP is expressed in select groups of hippocampal neurons, including the HIPPs in the hilus (Choi et al., 2007), a group of neurons that provide feedback inhibition to the GCL. Thus, removal of STEP from the HIPPs was predicted to increase glutamatergic responsiveness in the HIPPs and increase their inhibitory output. Our data are consistent this prediction by showing that STEP deficits lead to reduced potentiation of excitatory responses in the GCL.

Calcium imaging of responsiveness in GCL and hilus

These results were supported by the imaging data. When we measured peak fluorescence in the GCL from WT neurons, we found significantly larger values compared to those from the GCL of STEP KO neurons. Peak fluorescence, defined as the mean of the largest 1-second deflection in the stimulus interval, seemed to represent the responsiveness that could be seen in the raw data (compare Fig. 3A to Fig. 3Bi). However, for cases where the numbers of neurons responding to the stimulus were very low compared to the total number of neurons, then these measurements were marred by overwhelming noise from non-responders. This was almost always the case when measuring responses from the hilus, especially from WT slices, where very low numbers could be seen as responding in the hilus (Fig. 3C). We therefore added a measure of the proportion of responders, and we used criteria that would produce no false negatives, as there seemed to be little danger of a ceiling effect whereby all neurons might be classified as responding. Indeed, the highest measured proportion for any experiment was 0.79, found in one STEP KO slice in the GCL.

In taking the proportion data and mean peak fluorescence data together, we believe that these results are convincing given the following observation: compared to STEP KOs, the responses were generally greater in GCL for WT slices, while they were less in the hilar regions of WT slices—all from the same stimuli in the same slices. Thus, these results could not be explained by simple differences in the strength of stimulation or overall responsiveness, as these differential responses were seen in the hilus and GCL within the same slices.

Electrophysiological measurements from single GCL granule cells

Voltage clamp results—In order to measure inhibition of granule cells directly, we repeated the same stimulation protocol and measured responsiveness in individual GCL granule cells using voltage clamp recordings. The latencies of these IPSCs were identical for WT and STEP KO slices, and the durations of these latencies (greater than 12 msec), are consistent with a multisynaptic circuit connecting the stimulus site in CA1 to the evoked IPSCs.

In order to isolate GABAergic responses, the cells were voltage clamped at +10 mV, and the electrodes contained a cesium gluconate solution in order to block potassium conductances, which would otherwise produce large leak currents. In contrast to what we expected, the size of the evoked IPSCs were similar in the STEP KO and WT mice, while the WT mice demonstrated a significant increase in stimulus 3 vs. stimulus 1 (Fig. 4). This result supports the calcium imaging experiments in that there is an increase in responsiveness in WT slices during the stimulation protocol; the greater action potential firings of GCL granule cells drive local GABAergic interneurons more strongly, providing the potentiated IPSCs that are measured here. However, this finding doesn't support the idea that the lack of potentiation seen in STEP KO slices is due to increased GABAergic inhibition relative to WT slices.

Cell-attached results—We performed cell-attached recordings to verify that the granule cells in STEP KO and WT slices were responding to the electrical stimuli with excitatory responses, consistent with what we measured in the calcium imaging experiments. Several recordings with large depolarizations and action potentials evoked by the stimulus provided this verification (Fig. 5). In a majority of responses, however, we measured hyperpolarizations during the stimulus (Fig. 6). In comparing all hyperpolarizing stimulations between STEP KO and WT cells, we found the STEP KO responses to be significantly more hyperpolarized than the WT responses ($p<0.04$).

The cell-attached results contrast with the voltage clamp recordings where no significant differences between the WT vs. STEP KO granule neurons were found. One explanation for the differences in the two approaches to measure inhibition is that the voltage clamp recordings precluded measurements of GABA-B mediated potassium currents. GABA-B receptors are expressed strongly in the dendrites of GCL granule cells (Sloviter et al., 1999). Blocking GABA-B responsiveness in the voltage clamp recordings may have reduced a large component of dendritic GABAergic inhibition, resulting in recordings that were biased towards somatic GABAergic inhibition.

Conclusions

We propose the hypothesis that HIPP inhibitory input to GCL dendrites is stronger in STEP KO mice. With regards to the STEP KO mice vs. WT mice, this hypothesis can explain the larger seizure thresholds shown in the pilocarpine studies, the lack of potentiation in excitatory responses demonstrated in the calcium imaging studies, the lack of potentiation in GABA-A inhibitory responses shown in the voltage clamp data, and the larger putative GABA-B component shown in the cell-attached recordings. Future studies should confirm

whether HIPP neurons are indeed the source of greater inhibitory input in STEP KO mice, and confirm that the larger hyperpolarizations seen in STEP KO GCL neurons are derived from GABA-B responses.

Acknowledgments

Preliminary results from this work were presented earlier as an abstract (Briggs et al., 2007). We thank the members of our laboratories for helpful discussions and critical reading of the manuscript. We also thank Dmitriy Aronov and David Sussillo as the original authors of the macro that was modified for the imaging analysis in this study. This work was supported by: The Epilepsy Foundation (GA); the National Association of Research on Schizophrenia and Depression (NARSAD), NIH grants MH01527 and MH52711 (PJL) and an American Epilepsy Society Research Initiative Award (JRN). We confirm that we have read the Journal's position on issues involved in ethical publication and affirm that this report is consistent with those guidelines.

Abbreviations

STEP	STriatal Enriched protein tyrosine Phosphatase
STEP KO	STEP knockout
WT	STEP wild-type mice
SE	status epilepticus
HIPPs	hilar interneurons whose axons ramify in the perforant path (aka, somatostatin hilar interneurons)
GCL	granule cell layer of the dentate gyrus

References

Aaron G, Yuste R. Reverse optical probing (ROPING) of neocortical circuits. Synapse. 2006; 60:437–440. [PubMed: 16881073]

Acsady L, Kamondi A, Sik A, Freund T, Buzsaki G. GABAergic cells are the major postsynaptic targets of mossy fibers in the rat hippocampus. J Neurosci. 1998; 18:3386–3403. [PubMed: 9547246]

Baratta MV, Lamp T, Tallent MK. Somatostatin depresses long-term potentiation and Ca2+ signaling in mouse dentate gyrus. J Neurophysiol. 2002; 88:3078–3086. [PubMed: 12466431]

Bering R, Johansen FF. Expression of somatostatin mRNA and peptide in rat hippocampus after cerebral ischemia. Regul Pept. 1993; 49:41–48. [PubMed: 7904082]

Boulanger LM, Lombroso PJ, Raghunathan A, During MJ, Wahle P, Naegele JR. Cellular and molecular characterization of a brain-enriched protein tyrosine phosphatase. J Neurosci. 1995; 15:1532–1544. [PubMed: 7869116]

Braithwaite SP, Adkisson M, Leung J, Nava A, Masterson B, Urfer R, Oksenberg D, Nikolich K. Regulation of NMDA receptor trafficking and function by striatal-enriched tyrosine phosphatase (STEP). Eur J Neurosci. 2006a; 23:2847–2856. [PubMed: 16819973]

Braithwaite SP, Paul S, Nairn AC, Lombroso PJ. Synaptic plasticity: one STEP at a time. Trends Neurosci. 2006b; 29:452–458. [PubMed: 16806510]

Briggs SW, Choi YS, Aaron G, Austin D, Lin SL, Lombroso PJ, Obrietan K, Naegele JR. Role of STEP in hippocampal GABAergic interneuron death in pilocarpine-induced status epilepticus. Society for Neuroscience. 2007 Abstract.

Buckmaster PS, Jongen-Relo AL. Highly specific neuron loss preserves lateral inhibitory circuits in the dentate gyrus of kainate-induced epileptic rats. J Neurosci. 1999; 19:9519–9529. [PubMed: 10531454]

Buckmaster PS, Yamawaki R, Zhang GF. Axon arbors and synaptic connections of a vulnerable population of interneurons in the dentate gyrus in vivo. J Comp Neurol. 2002; 445:360–373. [PubMed: 11920713]

Choi YS, Lin SL, Lee B, Kurup P, Cho HY, Naegele JR, Lombroso PJ, Obrietan K. Status epilepticus-induced somatostatinergic hilar interneuron degeneration is regulated by striatal enriched protein tyrosine phosphatase. J Neurosci. 2007; 27:2999–3009. [PubMed: 17360923]

de Lanerolle NC, Kim JH, Robbins RJ, Spencer DD. Hippocampal interneuron loss and plasticity in human temporal lobe epilepsy. Brain Res. 1989; 495:387–395. [PubMed: 2569920]

Freund TF, Buzsaki G, Leon A, Somogyi P. Hippocampal cell death following ischemia: effects of brain temperature and anesthesia. Exp Neurol. 1990; 108:251–260. [PubMed: 1693578]

Han ZS, Buhl EH, Lorinczi Z, Somogyi P. A high degree of spatial selectivity in the axonal and dendritic domains of physiologically identified local-circuit neurons in the dentate gyrus of the rat hippocampus. Eur J Neurosci. 1993; 5:395–410. [PubMed: 8261117]

Johansen FF, Zimmer J, Diemer NH. Early loss of somatostatin neurons in dentate hilus after cerebral ischemia in the rat precedes CA-1 pyramidal cell loss. Acta Neuropathol (Berl). 1987; 73:110–114. [PubMed: 2885998]

Kobayashi M, Buckmaster PS. Reduced inhibition of dentate granule cells in a model of temporal lobe epilepsy. J Neurosci. 2003; 23:2440–2452. [PubMed: 12657704]

Kurup P, Zhang Y, Venkitaramani DV, Lombroso PJ. The role of STEP in Alzheimer's disease. Channels. 2010a; 4:1–4.

Kurup P, Zhang Y, Xu J, Venkitaramani DV, Haroutunian V, Greengard P, Nairn AC, Lombroso PJ. Abeta-mediated NMDA receptor endocytosis in Alzheimer's disease involves ubiquitination of the tyrosine phosphatase STEP61. J Neurosci. 2010b; 30:5948–5957. [PubMed: 20427654]

Lombroso PJ, Naegele JR, Sharma E, Lerner M. A protein tyrosine phosphatase expressed within dopaminoceptive neurons of the basal ganglia and related structures. J Neurosci. 1993; 13:3064–3074. [PubMed: 8331384]

Loscher W. Animal models of epilepsy for the development of antiepileptogenic and disease-modifying drugs. A comparison of the pharmacology of kindling and post-status epilepticus models of temporal lobe epilepsy. Epilepsy Res. 2002; 50:105–123. [PubMed: 12151122]

Lowenstein DH, Thomas MJ, Smith DH, McIntosh TK. Selective vulnerability of dentate hilar neurons following traumatic brain injury: a potential mechanistic link between head trauma and disorders of the hippocampus. J Neurosci. 1992; 12:4846–4853. [PubMed: 1464770]

MacLean JN, Watson BO, Aaron GB, Yuste R. Internal dynamics determine the cortical response to thalamic stimulation. Neuron. 2005; 48:811–823. [PubMed: 16337918]

Mathern GW, Babb TL, Leite JP, Pretorius K, Yeoman KM, Kuhlman PA. The pathogenic and progressive features of chronic human hippocampal epilepsy. Epilepsy Res. 1996; 26:151–161. [PubMed: 8985697]

Mathern GW, Babb TL, Pretorius JK, Leite JP. Reactive synaptogenesis and neuron densities for neuropeptide Y, somatostatin, and glutamate decarboxylase immunoreactivity in the epileptogenic human fascia dentata. J Neurosci. 1995; 15:3990–4004. [PubMed: 7751960]

Munoz JJ, Tarrega C, Blanco-Aparicio C, Pulido R. Differential interaction of the tyrosine phosphatases PTP-SL, STEP and HePTP with the mitogen-activated protein kinases ERK1/2 and p38alpha is determined by a kinase specificity sequence and influenced by reducing agents. Biochem J. 2003; 372:193–201. [PubMed: 12583813]

Nguyen TH, Liu J, Lombroso PJ. Striatal enriched phosphatase 61 dephosphorylates Fyn at phosphotyrosine 420. J Biol Chem. 2002; 277:24274–24279. [PubMed: 11983687]

Paul S, Nairn AC, Wang P, Lombroso PJ. NMDA-mediated activation of the tyrosine phosphatase STEP regulates the duration of ERK signaling. Nat Neurosci. 2003; 6:34–42. [PubMed: 12483215]

Pelkey KA, Askalan R, Paul S, Kalia LV, Nguyen TH, Pitcher GM, Salter MW, Lombroso PJ. Tyrosine phosphatase STEP is a tonic brake on induction of long-term potentiation. Neuron. 2002; 34:127–138. [PubMed: 11931747]

Perkins KL. Cell-attached voltage-clamp and current-clamp recording and stimulation techniques in brain slices. J Neurosci Methods. 2006; 154:1–18. [PubMed: 16554092]

Rafiq A, DeLorenzo RJ, Coulter DA. Generation and propagation of epileptiform discharges in a combined entorhinal cortex/hippocampal slice. J Neurophysiol. 1993; 70:1962–1974. [PubMed: 8294965]

Robbins RJ, Brines ML, Kim JH, Adrian T, de LN, Welsh S, Spencer DD. A selective loss of somatostatin in the hippocampus of patients with temporal lobe epilepsy. Ann Neurol. 1991; 29:325–332. [PubMed: 1675046]

Sanchez-Vives MV, McCormick DA. Cellular and network mechanisms of rhythmic recurrent activity in neocortex. Nat Neurosci. 2000; 3:1027–1034. [PubMed: 11017176]

Santhakumar V, Ratzliff AD, Jeng J, Toth Z, Soltesz I. Long-term hyperexcitability in the hippocampus after experimental head trauma. Ann Neurol. 2001; 50:708–717. [PubMed: 11761468]

Sloviter RS. Decreased hippocampal inhibition and a selective loss of interneurons in experimental epilepsy. Science. 1987; 235:73–76. [PubMed: 2879352]

Sloviter RS, li-Akbarian L, Elliott RC, Bowery BJ, Bowery NG. Localization of GABA(B) (R1) receptors in the rat hippocampus by immunocytochemistry and high resolution autoradiography, with specific reference to its localization in identified hippocampal interneuron subpopulations. Neuropharmacology. 1999; 38:1707–1721. [PubMed: 10587087]

Smetters D, Majewska A, Yuste R. Detecting action potentials in neuronal populations with calcium imaging. Methods. 1999; 18:215–221. [PubMed: 10356353]

Snyder EM, Nong Y, Almeida CG, Paul S, Moran T, Choi EY, Nairn AC, Salter MW, Lombroso PJ, Gouras GK, Greengard P. Regulation of NMDA receptor trafficking by amyloid-beta. Nat Neurosci. 2005; 8:1051–1058. [PubMed: 16025111]

Tallent MK, Siggins GR. Somatostatin acts in CA1 and CA3 to reduce hippocampal epileptiform activity. J Neurophysiol. 1999; 81:1626–1635. [PubMed: 10200199]

Thind KK, Yamawaki R, Phanwar I, Zhang G, Wen X, Buckmaster PS. Initial loss but later excess of GABAergic synapses with dentate granule cells in a rat model of temporal lobe epilepsy. J Comp Neurol. 2010; 518:647–667. [PubMed: 20034063]

Turski WA, Cavalheiro EA, Schwarz M, Czuczwar SJ, Kleinrok Z, Turski L. Limbic seizures produced by pilocarpine in rats: behavioural, electroencephalographic and neuropathological study. Behav Brain Res. 1983a; 9:315–335. [PubMed: 6639740]

Turski WA, Czuczwar SJ, Kleinrok Z, Turski L. Cholinomimetics produce seizures and brain damage in rats. Experientia. 1983b; 39:1408–1411. [PubMed: 6140182]

Venkitaramani DV, Paul S, Zhang Y, Kurup P, Ding L, Tressler L, Allen M, Sacca R, Picciotto MR, Lombroso PJ. Knockout of STriatal enriched protein tyrosine phosphatase in mice results in increased ERK1/2 phosphorylation. Synapse. 2009; 63:69–81. [PubMed: 18932218]

Zhang Y, Venkitaramani DV, Gladding CM, Zhang Y, Kurup P, Molnar E, Collingridge GL, Lombroso PJ. The tyrosine phosphatase STEP mediates AMPA receptor endocytosis after metabotropic glutamate receptor stimulation. J Neurosci. 2008; 28:10561–10566. [PubMed: 18923032]

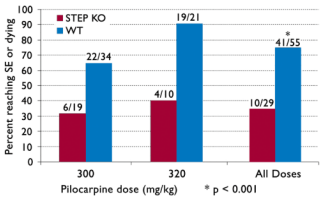

Figure 1. Percentage of mice reaching SE vs. pilocarpine dosage

The number of mice corresponding to the percent values in the y-axis are listed above each bar. The p-value was calculated using a Chi-square test for the equality of distributions.

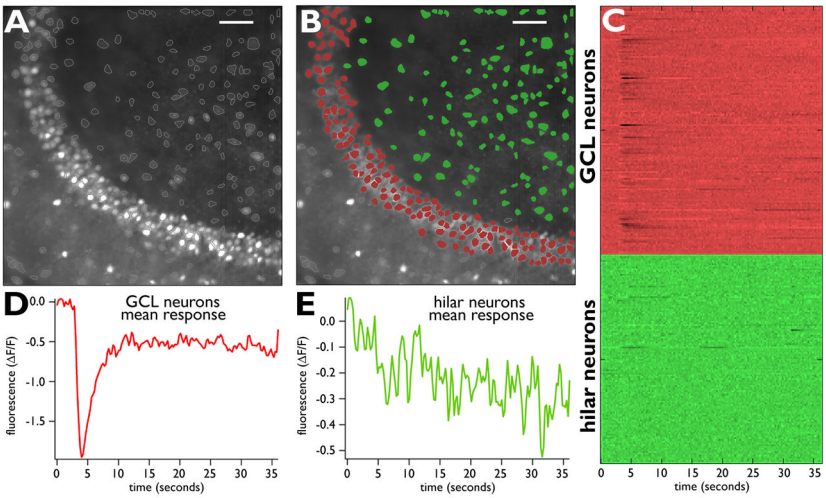

Figure 2. Calcium imaging in the dentate gyrus: an example

(A) Average movie frame from 36-second movie of the GCL and hilus from a single WT slice. Cell bodies labeled with fura-2 were identified by our software. (B) The borders of the GCL and hilus were identified manually and the cell bodies are colored red and green, respectively. (C) Raster plot of all neuronal calcium activity in these two regions. Each line represents one neuron, and each color represents the corresponding region of the slice. Darker transients indicate increased calcium influx, thus, high action potential activity. (D) Average response of GCL neurons. The response of all identified GCL neurons (labeled red in *B*) is shown as the average response. The response was produced by 60 shocks at 60 Hz, each shock being 0.1 msec and −4.0 mA in amplitude. The stimuli were applied to the Schaffer collaterals after 3-seconds of baseline. The peak shown in *D* is a measure of the mean response of the observed GCL neurons. (E) Same format as *D*, except that the mean response of all hilar neurons is shown. Scale bar in *A* and *B*: 50 μm.

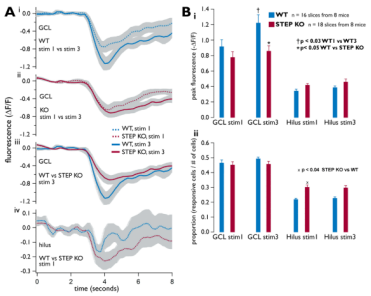

Figure 3. GCL and hilus calcium transients evoked during ictal-like stimulation of the hippocampal slice are significantly different

As in Fig. 2, the Schaffer collaterals were stimulated with tetanic stimulation. For all panels, plots are mean ± SE, n = 16 slices from 8 WT mice and n = 18 slices from 8 STEP KO mice. All WT results are shown in red, STEP KO in blue. (A) Mean 8-second long calcium transients from all slices. Each colored trace represents the mean transient from each indicated group (i.e., GCL, WT, stim1 as one group), and each group is com posed of the mean ΔF/F transients recorded from each slice (as in Fig. 2D and E). Grey shadings show the standard error of the mean traces. (B) Peak 1-second calcium transients. (i) The mean 1-second peak difference of GCL transients between stimulus 1 and stimulus 3 was significant in WT slices ($p<0.03$), and the same measured difference between WT and STEP KO slices was significant at stimulus 3 ($p<0.05$). (ii) Mean responsiveness is displayed, measured as the proportion of neurons responding to a stimulus. A significant difference between WT and STEP KO responsiveness in the hilus is shown ($p<0.04$).

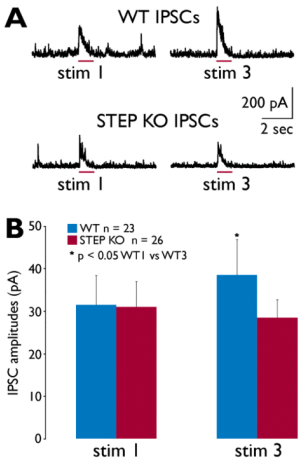

Figure 4. IPSCs recorded from GCL granule cells during Shaffer collateral stimulation

(A) Representative examples of IPSCs evoked from WT (top) and STEP KO slices. Granule cells were voltage-clamped at +10 mV with a cesium-gluconate intracellular solution to block potassium conductances. All outward (positive) currents are most likely due to GABA-A ionotropic currents in these recordings. The timing of the 1-second stimulus is indicated by the red bar for each trace. (B) Mean IPSC amplitudes were calculated from 23 WT and 26 STEP KO recordings. Mean IPSC amplitudes increased significantly between stimulus 1 and 3 for the WT recordings ($p<0.05$, paired t-test).

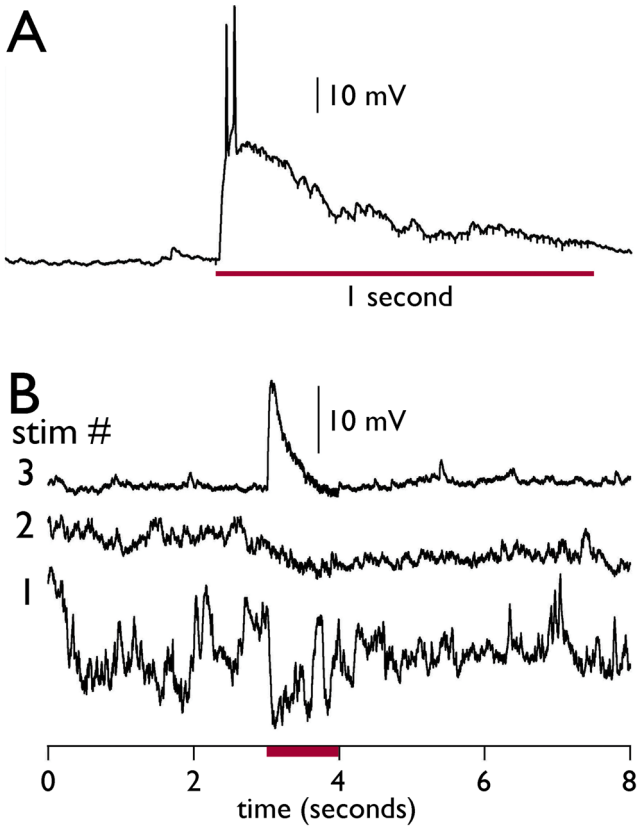

Figure 5. Cell-attached recordings of GCL granule cells during Shaffer collateral stimulation

Tight-seal cell-attached recordings allow some measure of the changes in membrane potential that occur in a single granule cell. (A) A large depolarization with action potentials in a single STEP KO granule cell is evoked by the same stimulus applied in the calcium imaging experiments (60 Hz train, 1-second duration). (B) This WT granule cell recording shows a hyperpolarizing response in stimulus 1 that becomes a strong depolarizing response in stimulus 3. The timing of the stimulus is indicated by the red bar.

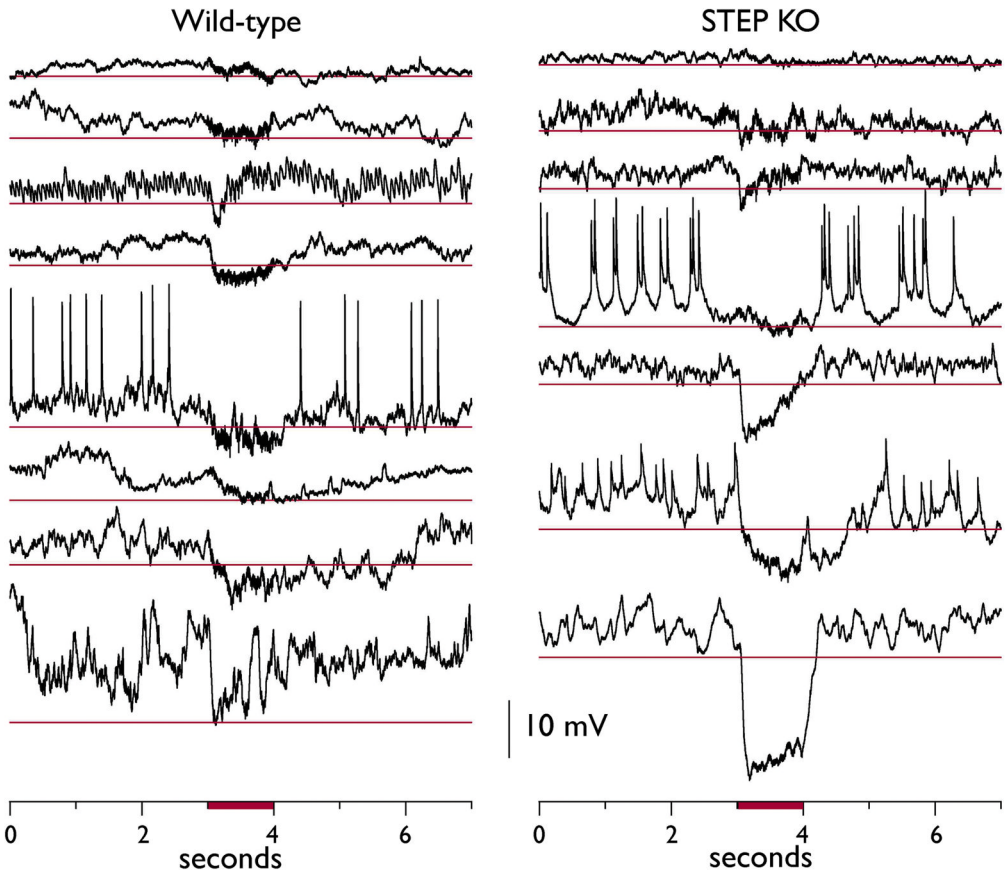

Figure 6. Cell-attached recordings of GCL granule cells demonstrate large hyperpolarizing responses in STEP KO slices

Only stimulus 1 responses that displayed a putative hyperpolarizing response to the stimulus are shown here. Examples from WT slices are shown on the left, and STEP KO slices on the right. The thin red lines for each recording represent the 99% confidence interval calculated from the 3-seconds of baseline potentials before each respective stimulus (not including presumed action potentials). The timing of the stimulus is indicated by the red bar.